Real-time synchrotron x-ray studies of low- and high-temperature nitridation of *c*-plane sapphire

Yiyi Wang,[1] Ahmet S. Özcan,[1] Gözde Özaydin,[2] Karl F. Ludwig, Jr.,[1] Anirban Bhattacharyya,[3]
Theodore D. Moustakas,[3] Hua Zhou,[4] Randall L. Headrick,[4] and D. Peter Siddons[5]

[1]*Physics Department, Boston University, Boston, Massachusetts 02215, USA*
[2]*Department of Aerospace and Mechanical Engineering, Boston University, Boston, Massachusetts 02215, USA*
[3]*Department of Electrical and Computer Engineering, Boston University, Boston, Massachusetts 02215, USA*
[4]*Department of Physics, University of Vermont, Burlington, Vermont 05405, USA*
[5]*National Synchrotron Light Source, Brookhaven National Laboratory, Upton, New York 11973, USA*

The plasma nitridation kinetics of *c*-plane sapphire at both low (200–300 °C) and high (750 °C) substrate temperatures was examined using grazing-incidence real-time x-ray diffraction, *in situ* x-ray reflection and *in situ* reflection high-energy electron diffraction (RHEED). These monitored the evolution of the nitride thickness, strain, and surface structure during nitridation. The evolution of the AlN($10\bar{1}0$) peak showed that the heteroepitaxial strain in the first layer of nitride is already significantly relaxed relative to the substrate. Subsequent layers grow with increasing relaxation. In both the high- and low-temperature nitridation cases, the results suggest that the early stage nitridation is governed by a complex nucleation and growth process. Nitridation at both temperatures apparently proceeds in a two-dimensional growth mode with the initial nucleating islands consisting of several monolayers which grow laterally. At low temperature the growth slows or even stops after impingement of the nucleating islands covering the surface, possibly due to low diffusivities through the existing layer. Initial formation and growth rates of nucleating islands at high temperatures are comparable to those at low temperatures, but subsequent growth into the substrate is significantly enhanced over the low temperature case, consistent with activation energies of 0.1–0.25 eV.

I. INTRODUCTION

The III-V nitrides have a variety of applications in blue light-emitting diodes, blue laser diodes, and other optoelectronic devices due to their wide direct band gap. However the lack of readily available good quality GaN substrates requires heteroepitaxial growth of GaN thin films on other substrates, such as Si, SiC, and most commonly sapphire. There is an approximately 16% mismatch between sapphire and GaN lattice spacing. Therefore the proper preparation of the sapphire surface prior to GaN deposition is crucial. Typically, the treatment of the sapphire surface by a nitrogen plasma or an ammonia source is utilized to produce a chemical reaction between the sapphire surface and nitrogen and convert the surface to relaxed AlN.[1,2] The characteristics of the nitridated layer, such as coverage, structure, and thickness strongly influence the quality of the subsequent nitride epilayer growth and the resulting film properties, such as mobility and luminescence.[3] Recent studies[4–6] show that the substrate temperature during nitridation plays an important role in growing good quality GaN epilayers. Although high temperatures have been preferred for nitridation to enhance the reactivity of nitrogen, the production of active nitrogen species by plasma sources has allowed low temperature nitridation to be considered as an alternative. Several groups have reported that 200 °C nitridation produces a homogeneous AlN layer on the sapphire substrate with improved structural and optical properties of the GaN epilayer.[4,5] In addition to the substrate temperature, the nitridation kinetics may show strong dependence on external factors, such as the plasma source, nitrogen gas purity, and chamber cleanliness. Not only different types of plasma sources, such as electron cyclotron resonance (ECR) vs radio frequency (RF), produce different kinds of active nitrogen species, but also different initiations of the plasma for the same source may affect the flux ratio of the plasma species.[7,8]

Several x-ray photoelectron spectroscopy (XPS) studies have examined the growth kinetics of the nitridation layer.[9–12] While XPS gives a signal proportional to the near-surface chemical concentrations, it is difficult to make a clear calibration between signal level and effective film thickness. Moreover, XPS is totally insensitive to the crystallographic state of the chemical species in question and usually operates in a mode in which the nitridation process is stopped for measurement. Thus the kinetic record reported is relatively sparse in time.

Here we report a detailed real-time surface-sensitive x-ray scattering study examining the temporal evolution of the nitridated layer thickness. The equivalent film thickness is calibrated by x-ray reflectivity measurements. The formation of the AlN structure at the surface is also verified by *in situ* reflection high-energy electron diffraction (RHEED).

II. EXPERIMENT

Real-time grazing-incidence surface-sensitive x-ray experiments were performed in a custom surface x-ray ultra-high vacuum chamber (10^{-9} torr base pressure) installed at beamline X21 of the National Synchrotron Light Source (NSLS) at Brookhaven National Laboratory (BNL). More details about this real-time surface x-ray characterization facility for dynamic processing are described elsewhere.[13] An incident photon energy was chosen between 10.40 keV and 11.04 keV for individual samples with a flux of 2×10^{12}
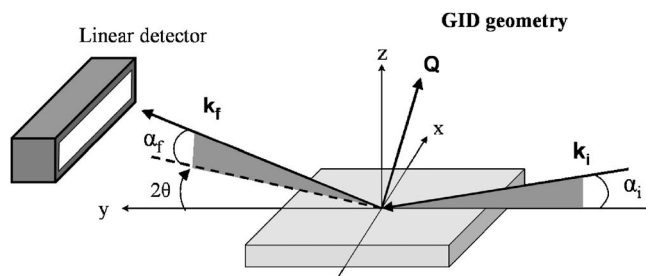
FIG. 1. Schematic of the x-ray grazing incidence diffraction geometry. Wave vectors k_i and k_f are the incident and scattered wave vectors, respectively; Q is the momentum transfer defined by α_i, α_f and in-plane angle 2θ. The linear position-sensitive detector is oriented parallel to the sample surface.

photons per second using a nondispersive Si(111) double-crystal monochromator with a beam size of 0.5 mm $\times$ 0.5 mm at a storage ring current of 300 mA.

Results from three samples will be shown, which we label as samples A, B, and C. Sample A was nitridated at 300° for 180 min, sample B was nitridated at 750 °C for 195 min, and sample C was nitridated at 200° for 155 min. For all nitridation experiments, ultrahigh purity (UHP) grade nitrogen (99.999% purity) was used. In addition, a nitrogen gas purifier from Mykrolis Corporation was installed at the plasma source gas inlet to obtain a higher purity level of nitrogen. The experiments with samples A and B were performed at a different synchrotron run than those for sample C. Although the same sample preparation and nitridation procedures were used at the different experimental runs, the nitrogen plasma and ambient impurity conditions could be slightly different. According to our procedures, the c-plane sapphire samples were first outgassed at 800 °C in the UHV process chamber. The temperature was then reduced for the nitridation process. A UNI-Bulb RF plasma source from Applied Epi–Veeco operated at 300 W was used to obtain active nitrogen. The nitrogen flow rate was between 0.4 and 0.8 sccm and the chamber pressure was approximately 1 $\times 10^{-5}$ Torr during nitridation.

After outgassing and prior to nitridation, RHEED and x-ray reflectivity measurements were performed as a baseline. The x-ray geometry used in our experiments is shown in Fig. 1. The diffracted intensity was collected by a one-dimensional (1D) position sensitive detector (PSD) mounted in a vertical geometry. For the grazing incidence diffraction (GID) measurements, both the incidence angle α_i and exit angle α_f were kept constant at approximately 0.5° to enhance surface sensitivity. For samples A and B the AlN in-plane $(10\bar{1}0)$ peak intensity was monitored by a series of x-ray rocking scans in real time during the subsequent nitridation process. In order to examine the surface structure, AlN coverage and strain relaxation, the nitridation process was interrupted for RHEED, x-ray reflectivity, and radial x-ray GID measurements every 30 min. The in-plane radial GID scans were performed along the AlN$[l0\bar{l}0]$ direction, which includes the angular range of the sapphire $(11\bar{2}0)$ peak and AlN$(10\bar{1}0)$ peak. Sample C was studied in the same manner as samples A and B, however, without the in-plane GID

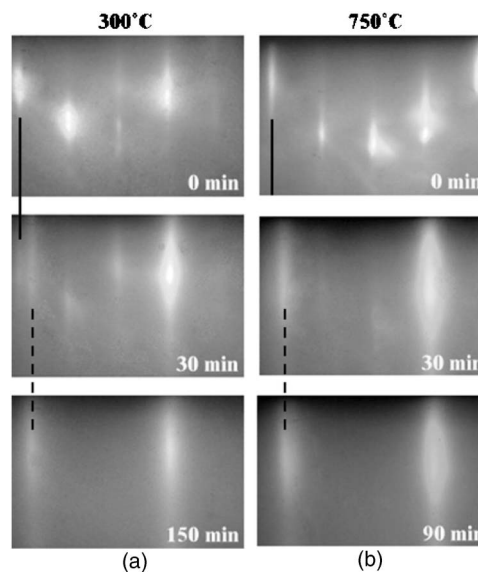

FIG. 2. (a) RHEED patterns of sample A along the sapphire $\langle 11\bar{2}0 \rangle$ azimuth. The in-plane direction of the AlN layer is rotated 30° with respect to the sapphire direction, such that $[11\bar{2}0]$AlN $\parallel[10\bar{1}0]$ sapphire. The solid line indicates the sapphire streak; the dashed line indicates the AlN streak. (b) RHEED patterns of sample B along the sapphire $\langle 11\bar{2}0 \rangle$ azimuth.

scans along $(l0\bar{l}0)$. Instead the AlN in-plane $(10\bar{1}0)$ peak intensity of sample C was monitored in real time with 5 s resolution with no rocking scans. *Ex situ* atomic force microscopy (AFM) measurements were carried out to characterize the surface morphology of the nitridated samples, using a Digital Instruments Nanoscope D3000 operating in tapping mode.

III. RESULTS

A. Sample A (300 °C nitridation)

Figure 2(a) shows the *in situ* RHEED patterns of sample A along the sapphire $\langle 11\bar{2}0 \rangle$ azimuth. The streaky RHEED pattern of the degassed sapphire substrate indicates a smooth unreconstructed surface. New streaks appear among the sapphire rods after 30 minutes of nitridation. These streaks, indicated by the dashed line, correspond to the AlN$\{11\bar{2}0\}$ diffraction lines. This typical epitaxial alignment indicates that the AlN$[11\bar{2}0]$ direction is rotated 30° with respect to the sapphire $[11\bar{2}0]$ direction.[14] After a total time of 150 min, the sapphire streaks disappear completely. The remaining AlN streaks suggest that the sapphire surface is converted into an AlN layer after nitridation.

The selected x-ray reflectivity scans of sample A are plotted in Fig. 3(a) after geometric corrections. The reflectivity intensities are corrected by a factor of inverse $\sin(\alpha_i)$ because the projected length of the x-ray beam on the sample at grazing incidence angle is longer than the sample. The oscillations in the reflectivity are due to the constructive and destructive interference of waves reflected at the surface and
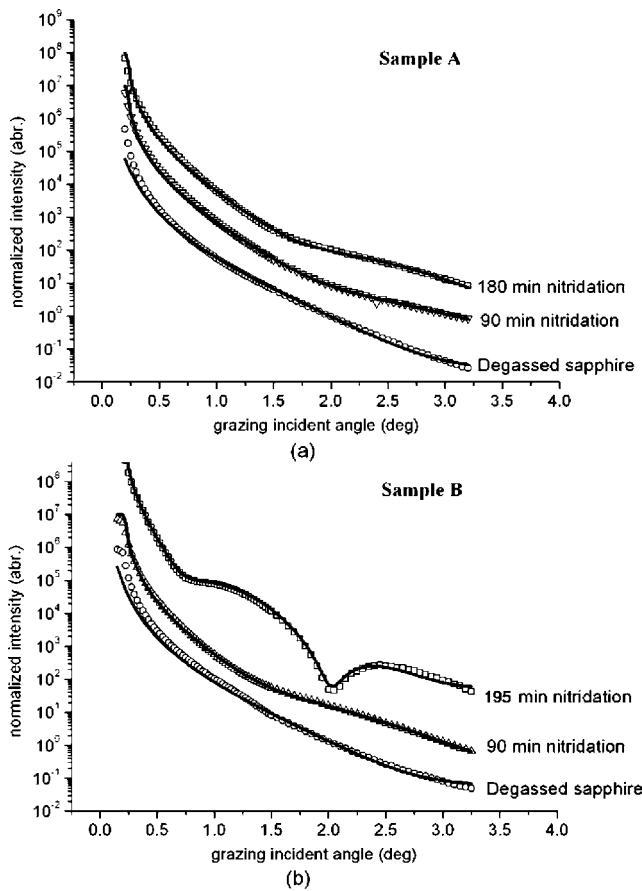
FIG. 3. (a) Reflectivity curves of sample A (300 °C growth) before nitridation, after 90 min and after 180 min of nitridation are plotted (curves are translated vertically for clarity). Open symbols show the experimental data and the solid lines show the best-fit results. (b) Reflectivity curves of sample B (750 °C growth) before nitridation, after 90 min and after 195 min of nitridation are plotted.

the interface. The reflectivity data were fit using the formalism developed in Ref. 15 from the Fresnel equation and Born approximation. Open symbols show the experimental data and the solid lines represent the best-fit results. Table I displays the best fit results for film thickness, film electron density, surface roughness and interface roughness.

In order to examine the growth of the nitride layer in more detail, the AlN($10\bar{1}0$) peak intensity evolution was monitored by surface-sensitive GID measurements in real time during the nitridation process. Rocking scans at the AlN($10\bar{1}0$) peak were integrated to obtain an approximate measure of the volume fraction transformed into AlN. It took 3.73 min to complete and restart each rocking scan. The rate of the nitridation was sufficiently slow that no significant evolution was missed during the scanning time. The integrated intensities are approximately proportional to the volume of AlN material and are converted to equivalent film thickness using the reflectivity fit results. Figure 4(a) shows the time evolution of the AlN($10\bar{1}0$) peak intensity of sample A. Arrows indicate the interruption points for RHEED and reflectivity measurements at 30 min intervals. In order to maintain the plasma condition, the source remained on, but was shuttered during interruptions. As can be seen on the diffraction curves, the data show the existence of a brief transient behavior associated with each interruption of the nitridation process. When the nitridation process starts again following the interruption, the x-ray intensity is initially higher than it was when the nitridation had been stopped. However, there is a transient relaxation back to a level consistent with the observed intensity at the time the nitridation had been stopped. The transient period lasts for 10–15 min. The transient behavior becomes more significant at later stages of nitridation when the AlN layer is thicker. We speculate that this transient behavior may indicate smoothening of the surface when the plasma source is shuttered. When the shutter is then reopened, there is a return to a rougher dynamic growth state. The source of surface roughness during growth could be the nitrogen adatoms themselves or sputtering of the AlN surface by the nitrogen plasma.

In Fig. 4(a) the AlN peak intensity evolution shows two distinct regimes separated by a crossover region at a thickness ~10–12.5 Å (4–5 MLs) after a time 90–120 min. This is also observed by the electron density evolution from the reflectivity analysis shown in Fig. 5 and the radial GID measurement along the AlN[$l0\bar{l}0$] direction shown in Fig. 6(a). In the second regime, after about 120 min of total nitridation time, the growth rate slows simultaneously with the saturation of AlN electron density shown in Fig. 5. During the early and middle stages of the observed growth, the apparent AlN electron density is well below the bulk value. This suggests that layers growing on the sapphire are incomplete at this time. By the end of the nitridation, the fit result

TABLE I. Reflectivity best-fit results/parameters of sample A at 300 °C nitridation.

| Sample condition	Nitridated layer thickness (Å)	Nitridated layer electron density (cm^{-3})	Roughness (Å) sapphire-AlN	Roughness (Å) AlN-air
After outgassing	0	N/A	3.6	N/A
After 30 min of nitridation	1.3	3.0×10^{23}	3.8	3.6
After 60 min of nitridation	6.0	3.0×10^{23}	3.4	4.3
After 90 min of nitridation	9.1	2.7×10^{23}	3.0	2.7
After 120 min of nitridation	11.0	1.0×10^{24}	0	3.5
After 150 min of nitridation	13.0	1.1×10^{24}	0	4.0
After 180 min of nitridation	13.5	1.0×10^{24}	0	3.7
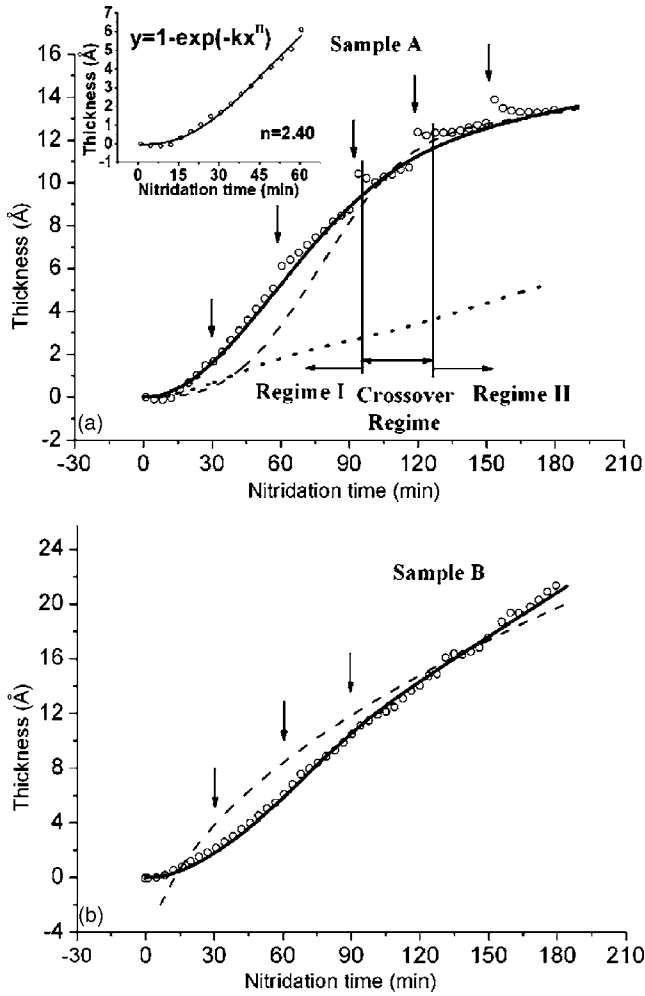
FIG. 4. (a) Time evolution of the AlN $(10\bar{1}0)$ peak intensity of sample A (300 °C growth). Arrows indicate the interruption points for reflectivity at 30 min intervals. The solid line represents the best fit with initial nucleating islands of 5 AlN ML thickness in the site-saturated nucleation and growth mode. The dashed line represents the fit with initial nucleating islands of 5 AlN ML thickness in the continuous nucleation and growth mode of the initial islands. Dotted line represents the fit with initial nucleation of one AlN ML in the site-saturated mode. The inset shows the best fit of the initial 60 min with the 2D JMAK model, which gives a growth exponent $n=2.40$. (b) Time evolution of the AlN $(10\bar{1}0)$ peak intensity of sample B (750 °C growth). The solid line represent the best fit with initial nucleating islands three AlN MLs thick. Dashed line represents the fit by a simple square-root growth function.

for the AlN electron density is near the bulk value, suggesting that layer formation is complete. This suggests that the slowdown in growth kinetics observed in the second regime may be due to the impingement of AlN islands growing laterally on the sapphire surface. This is modeled quantitatively in Sec. IV below.

As seen in Fig. 6(a), the initial AlN$(10\bar{1}0)$ peak is already partially relaxed from the fully strained epitaxial sapphire $(11\bar{2}0)$ position when it first forms. The AlN peak then shifts toward the bulk position from the partially relaxed position. However, the peak position does not reach the bulk value during the experimental period. The evolution of domain sizes and strain of the nitridated layer calculated from the AlN$(10\bar{1}0)$ peak widths and positions are shown in Fig. 7(a). Most of the strain relaxation takes place before the onset of the second regime, i.e., presumably during the lateral domain growth before impingement. The strain apparently saturates in the later part of second regime. The initial and final compressive strains are approximately 2.5% and 1.4%, respectively compared to the bulk AlN lattice constant.

The initial lateral domain size determined from the x-ray peak width is approximately 5.5 nm, but it increases to approximately 14.5 nm by the end of the experiment. As with the strain relaxation, the initial rate of change is rapid, but the process becomes slower, consistent with the decrease in overall film growth rate observed at late times in Fig. 4(a).

Ex situ AFM results of bare sapphire and sample A after 180 min nitridation are shown in Figs. 8(a) and 8(b), respectively. The surface morphology after nitridation is similar to that of bare sapphire, suggesting good conformity of the nitride layer. The RMS roughness from AFM analysis after nitridation is 2.2 Å.

B. Sample B (750 °C nitridation)

Figure 2(b) shows the *in situ* RHEED patterns of sample B along sapphire $\langle 11\bar{2}0 \rangle$ azimuth. The streaky RHEED pattern of the degassed sapphire substrate indicates a smooth unreconstructed surface. New streaks, corresponding to the AlN$\{11\bar{2}0\}$ diffraction lines, appear among the sapphire rods after 30 min. After a total nitridation time of 90 min, the sapphire streaks disappear completely. The remaining AlN streaks suggest that the sapphire surface is converted into an AlN layer after nitridation.

TABLE II. Reflectivity best-fit results/parameters of sample B at 750 °C nitridation.

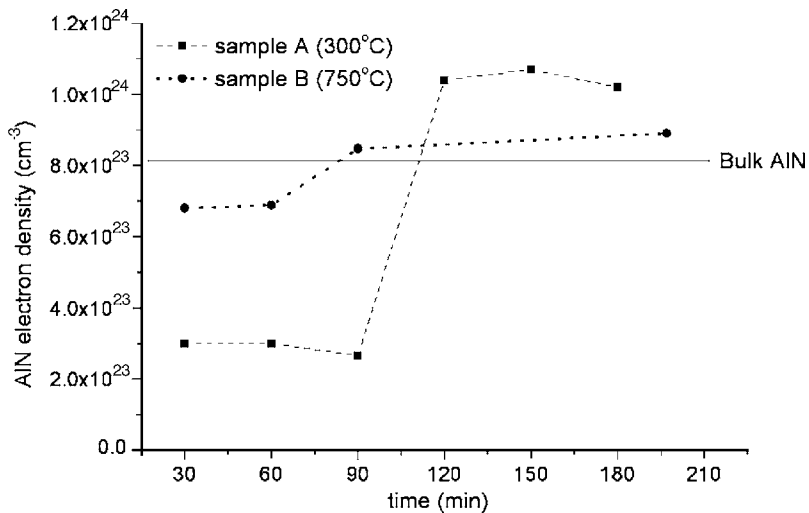| Sample condition	Nitridated layer thickness (Å)	Nitridated layer electron density (cm^{-3})	Roughness (Å) sapphire-AlN	Roughness (Å) AlN-air
After outgassing	0	N/A	3.7	N/A
After 30 min of nitridation	2.1	6.8×10^{23}	3.7	3.5
After 60 min of nitridation	6.1	6.9×10^{23}	4.8	2.2
After 90 min of nitridation	10.5	8.5×10^{23}	4.6	2.6
After 195 min of nitridation	25.3	8.9×10^{23}	2.7	5.0

FIG. 5. Electron density evolution vs time of samples A and B.

The x-ray reflectivity curves of sample B are shown in Fig. 3(b) after geometric corrections. Table II displays the best fit results of the reflectivity data. Sample B was examined in the same manner as sample A by real-time surface-sensitive radial GID measurements. In Fig. 5, the AlN electron density starts to saturate after approximately 90 min nitridation, suggesting that a complete layer is formed. This corresponds to a subtle change in slope seen in the time evolution of the AlN(10$\bar{1}$0) peak intensity of Fig. 4(b). The thicknesses at this these times are 7.5–12 Å(3–5 MLs). However, the nitridation continues at a significant rate, in contrast to the slowdown in growth rate observed in the low temperature case. Fitting results of this data is discussed in Sec. IV below.

As seen in Fig. 6(b), similar to the low temperature nitridation of sample A, the initial AlN peak indicates that the film is partially relaxed when it first forms. The peak then shifts toward the bulk position from the initial strained position, however again it does not reach the bulk value during the experimental period. Figure 7(b) shows that most of the strain relaxation of sample B at high temperature also takes place before the onset of the second regime as previously observed in sample A at low temperature. Again the evolution slows when the film reaches a certain thickness. The initial strain is approximately 2.2% relative to the bulk AlN value, which is a little lower than that of sample A (2.5%). The final strain is approximately 1.5%, which is a little higher than that of sample A (1.4%). However, a slow strain relaxation appears to be continuing even at the latest time studied here.

In contrast to the low temperature case, the peak width evolution indicates that average nitride domain size continues to increase significantly throughout the experiment. This might be due to coalescence of domains in subsequent layers. Nonetheless, the final domain sizes in the high- and low-temperature nitridation cases are similar.

The *ex situ* AFM topograph of sample B after nitridation exhibits small protrusions, as seen in Fig. 8(c). This might be due to the sputtering of the newly formed AlN by the few ionic species in the nitrogen plasma. However, the surface otherwise remains smooth and featureless despite a thicker coverage of AlN than was the case in the low temperature nitridation of sample A. The RMS roughness calculated from the AFM topograph after nitridation is 2.2 Å.

C. Sample C (200 °C nitridation)

The x-ray diffraction results of low temperature nitridation from sample C show only a slightly different behavior than sample A. Sample C was nitridated at a different synchrotron run, probably under a different plasma initiation and impurity level status. It was studied in the same manner as sample A, except that the AlN in-plane (10$\bar{1}$0) peak intensity was monitored in real time with 5 s resolution and without rocking scans. Figure 9 shows the reflectivity curves of sample C. The best-fit results are shown in Table III. As seen in Fig. 10, the x-ray diffraction data show two distinct regimes in the thickness evolution, similar to the behavior observed in the low-temperature nitridation of sample A. However, after the turning point at a thickness of ∼7.5 Å (3 AlN MLs), the peak continues to grow linearly into the succeeding layers instead of saturating as in the case of sample A. Nonetheless, the distinction between the two growth regimes is clear. The reflectivity fitting result shows that the electron densities after 75 min and 155 min nitridation are close to the bulk AlN value, which means the layer formation is already complete at those times. This is consistent as the turning point at ∼45 min observed in Fig. 10. As will be discussed in Sec. IV below, the total nitridation evolution could be fit by a two-dimensional (2D) nucleation and growth model with an initial nucleating layer consisting of 3 AlN MLs.

IV. DISCUSSION

A. Low temperature nitridation—growth kinetics

In their XPS studies of nitridation at 400 °C, Heinlein *et al.*[9] saw two distinct growth regimes: a linear increase followed by a saturation regime. They interpreted the observed turning point as the formation of a single AlN monolayer and attributed the change in the growth rate to the difficulty of breaking subsurface Al-O bonds after a full coverage is ob-
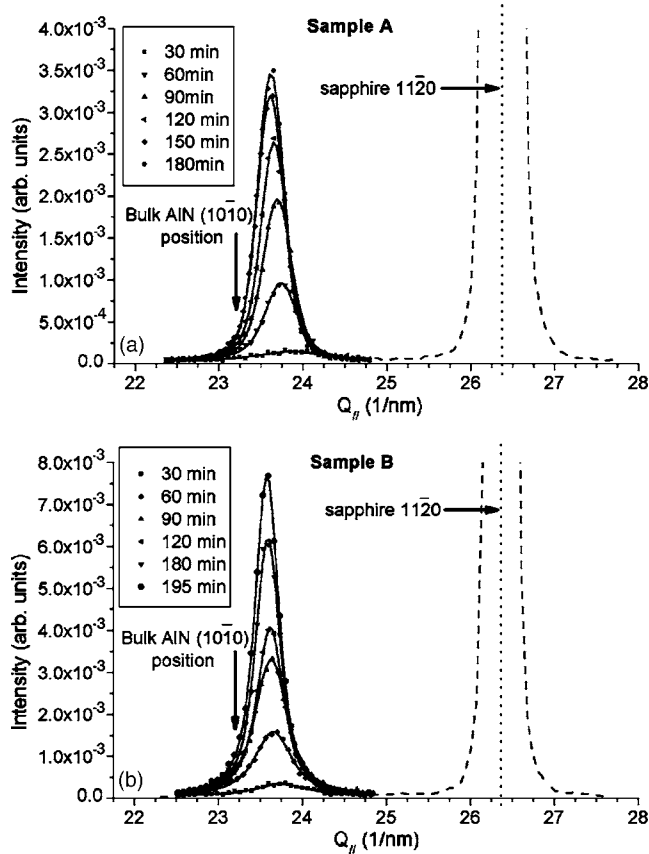
FIG. 6. (a) The x-ray GID pattern of sample A along the AlN $[l0\bar{l}0]$ direction at incident x-ray energy 10.4 keV. Various symbols show the experimental data at different nitridation time. The solid lines represent the best fit of a Voigt function to determine peak positions, heights and widths. The sapphire $(11\bar{2}0)$ peak is plotted in dashed line and the peak position is marked by a dotted line. (b) The x-ray GID pattern of sample B along the AlN $[l0\bar{l}0]$ direction at incident x-ray energy 10.4 keV.

FIG. 7. The evolution of domain size and strain relaxation during nitridation of (a) sample A and (b) sample B.

tained. This conclusion assumes that the unreconstructed sapphire surface is terminated by Al atoms and therefore surface nitridation beyond the first monolayer entails breaking of subsurface Al-O.[10,16] However, our x-ray data on low-temperature nitridation suggests the completion of several AlN MLs (i.e., 3–5 MLs) before the saturation or slowing of nitridation. In addition, the roughness of the surface does not increase significantly during nitridation, in contrast to the increase in surface roughness expected for the onset of protrusion growth suggested by Heinlein *et al.*[9]

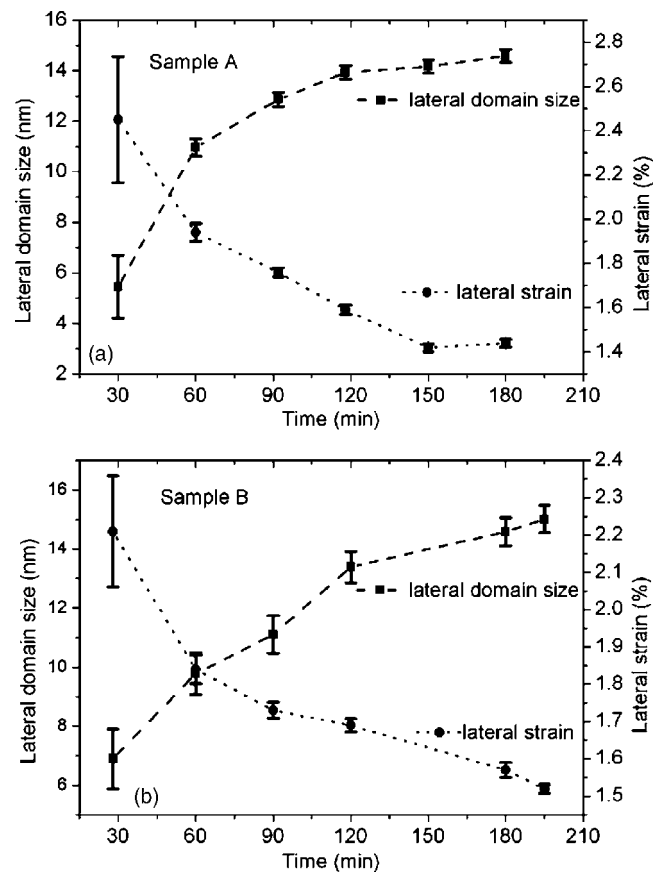Since the lateral size of islands is much larger than their thickness at the time of impingement, the growth process must be very anisotropic, with lateral growth occurring much more rapidly than vertical growth into the sapphire. In seeking to model the nucleation and growth kinetics of the AlN film, we therefore must examine models which incorporate this anisotropic behavior. For samples A and C, nitridated at 300 °C and 200 °C respectively, the initial growth curves rapidly upward in an exponential manner suggesting a nucleation process. The linear growth rate observed in the latter part of both data sets, however, suggests a constant (small) growth velocity normal to the surface. The very initial stage of the nitridation process can be fit well with a 2D Johnson-Mehl-Avrami-Kolmogorov (JMAK) model of nucleation and growth[17–19]

$$A(t) = 1 - \exp(-kt^n), \tag{1}$$

where A is the area fraction transformed, k is the rate constant, n is the growth exponent, and t is time. In general, both

TABLE III. Reflectivity best-fit results/parameters of sample C at 200 °C nitridation.

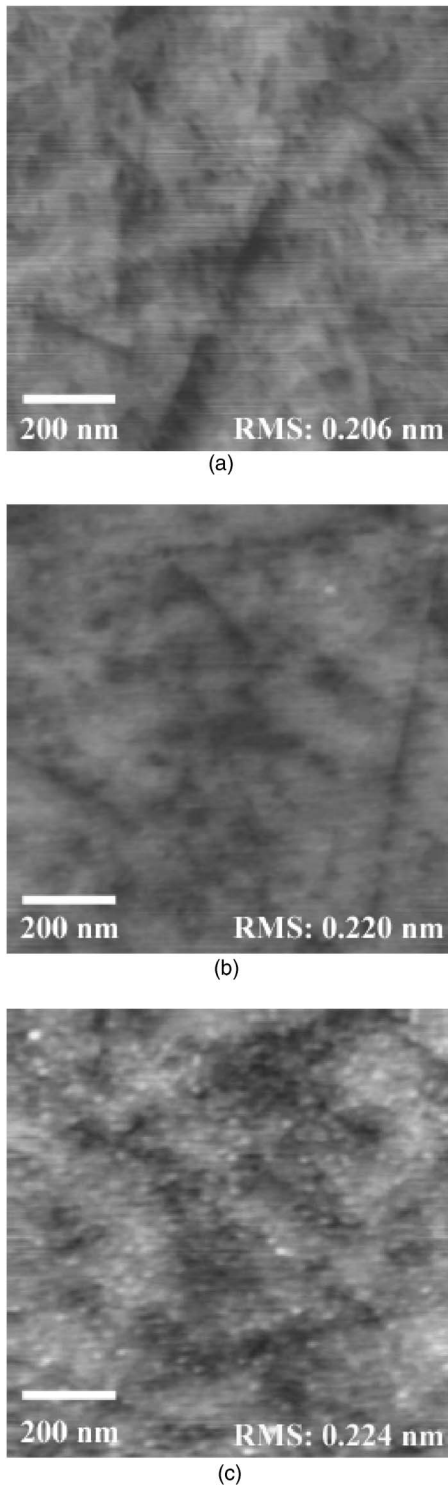| Sample condition	Nitridated layer thickness (Å)	Roughness (Å) sapphire-AlN	Roughness (Å) AlN-air
After outgassing	0	2.5	N/A
After 75 min of nitridation	8.5	3.3	2.7
After 155 min of nitridation	14.1	3.7	2.4

(a)

(b)

(c)

FIG. 8. AFM image of (a) bare sapphire, (b) sample A after 180 min of nitridation at 300 °C, (c) sample B after 195 min of nitridation at 750 °C.

k and n depend on the nature of nucleation and growth. For the nitridation of samples A and C, the best fit results of Eq. (1) [shown in the insets of Fig. 4(a) and Fig. 10, respectively] give growth exponents of $n=2.40$ for sample A and $n=2.67$ for sample C, which is intermediate between the exponents of $n=2$ and $n=3$ expected for a 2D growth with
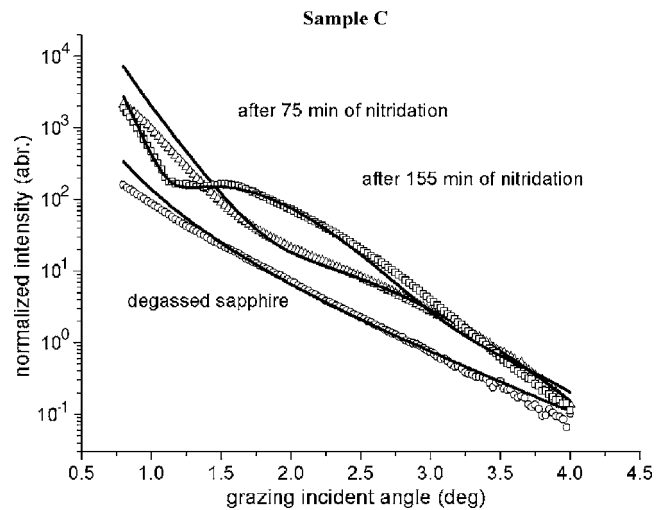

FIG. 9. Reflectivity curves of sample C (200 °C growth) before nitridation, after 75 min and after 155 min of nitridation are plotted. Open symbols show the experimental data and the solid lines represent the best-fit results.

site-saturated nucleation ($n=2$) and continuous nucleation ($n=3$). However since the nitridation process includes growth into the substrate, we must significantly modify the simple 2D JMAK model if we are to fit the entire growth process observed.

In order to perform a more detailed fit of the experimental curve, we created a simple model in which an initial set of AlN islands nucleates at random positions on the surface and grows laterally, as illustrated in Fig. 11 (top two images). These nucleating islands can be thicker than one monolayer deep—indeed this was essential to reproduce the data. We investigated models in which the initial set of nucleating islands develop only at time $t=0$ ("site-saturated nucleation"

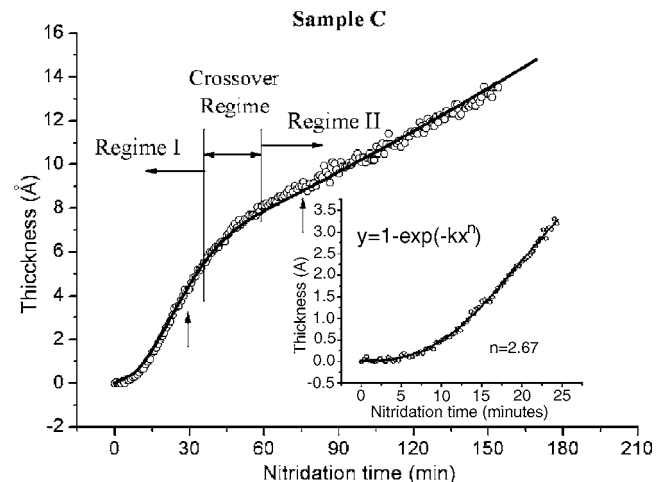FIG. 10. Time evolution of the AlN $(10\bar{1}0)$ peak intensity of sample C (200 °C growth). Arrows indicate the interruption points for reflectivity and RHEED at 25 min and 75 min. The solid line represents the best fit with initial nucleating islands of three AlN ML thickness. The insert shows the best-fit result of the 2D JMAK equation of the initial 25 min of nitridation, which gives a growth exponent $n=2.67$.

2-D site-saturated nucleation in the initial layer(s)

2-D continuous nucleation in the 2nd layer

2-D continuous nucleation in the 3rd layer

1 ML in initial nucleation layer
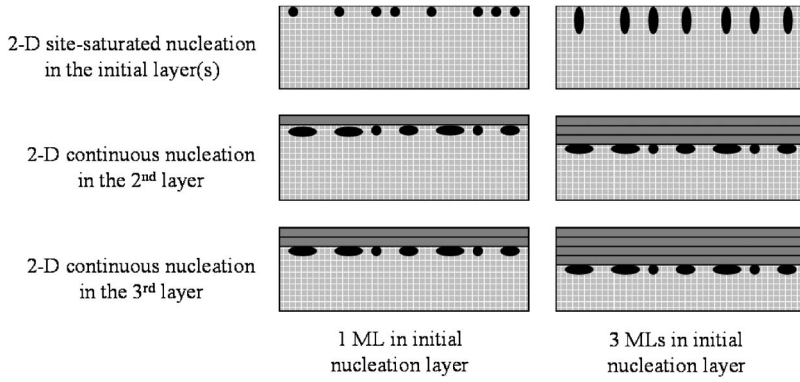
3 MLs in initial nucleation layer

FIG. 11. Nitridation nucleation models. Left column graphs show the nitridation nucleation model in a time sequence with 1 ML in the initial nucleating islands. Right column graphs show the nucleation model with 3 MLs in the initial nucleating islands. Top row graphs show 2D site-saturated nucleation in the initial layer(s); middle row graphs show 2D continuous nucleation in the second layer; bottom row graphs show 2D continuous nucleation in the third layer.

presumably due to nucleation occurring at specific defect sites on the surface) or instead can form continuously ("continuous nucleation") until the sapphire surface is fully consumed. We found that the best fitting results are obtained for the 2D site-saturated models and therefore describe their calculation. In the 2D JMAK model, the actual area fraction transformed in some interval is calculated from the extended area fraction transformed

$$dA = (1 - A)dA_{ext}. \qquad (2)$$

In the case of 2D site-saturated nucleation and growth where all nucleation happens at $t=0$, the change in the extended area fraction over the interval τ and $\tau + d\tau$ is

$$dA_{ext} = N \times 2\pi\nu_1^2 \tau d\tau, \qquad (3)$$

where N is the nuclei density per unit volume, and ν_1 is the growth velocity in the initial layer. On substituting into Eq. (2), we get

$$A(t) = 1 - \exp(-N\pi\nu_1^2 t^2). \qquad (4)$$

The volume fraction transformed at time t in the nucleating islands is therefore

$$V_{initial}(t) = dp\{1 - \exp(-N\pi\nu_1^2 t^2)\}, \qquad (5)$$

where p is the number of AlN monolayers in the nucleating islands and d is the thickness of one AlN monolayer (~ 2.5 Å).

As the AlN islands impinge on each other, the volume growth rate slows as in a traditional JMAK model. However the impingement of islands does not terminate the growth because nitridation continues through the growth of AlN into the subsurface layers. After this initial growth, our model assumes that subsequent vertical island growth into the sapphire is by the nucleation and growth of monolayers in a continuous mode, as shown in Fig. 11 (images in the middle row). Thus AlN monolayers can continuously nucleate under an existing AlN island at a fixed temporal rate per unit area, as shown in Fig. 11 (images in the bottom row). These additional layers will then grow laterally themselves. Subsequent AlN monolayers nucleate and grow in a similar manner. In this model, the abrupt change in slope observed in the data occurs when the lateral growth of the nucleating islands is complete. Ultimately the kinetics then essentially becomes that of 1D growth into the substrate.

To calculate the kinetics of these subsequent sublayers forming under the existing AlN islands, we consider the change in the extended area fraction in the mth sublayer due to nuclei which formed in the interval between τ and $\tau + d\tau$

$$dA_{ext}^m = M\pi\nu_2^2(t - \tau)^2 d\tau A^{m-1}(t), \qquad (6)$$

where M is the nucleation rate per unit volume per unit time, ν_2 is the growth velocity in the subsequent layers and A^{m-1} is the extended area fraction in layer above mth sublayer. On substituting into Eq. (2), we get the area fraction in the mth sublayer

$$A^m(t) = 1 - \exp\left\{-\int_0^t M\pi\nu_2^2(t - \tau)^2 A^{m-1}(t)d\tau\right\}. \qquad (7)$$

The total sum of volume fraction transformed in the m subsequent sublayers at time t is

$$V_{sub} = d\sum_{i=2}^{m}\left\{1 - \exp\left\{-\int_0^t M\pi\nu_2^2(t - \tau)^2 V^{i-1}(t)d\tau\right\}\right\}. \qquad (8)$$

Therefore the total volume fraction transformed during growth is the sum of Eqs. (5) and (8)

$$V_{tot} = dp\{1 - \exp(-N\pi\nu_1^2 t^2)\}$$
$$+ d\sum_{i=2}^{m}\left\{1 - \exp\left\{-\int_0^t M\pi\nu_2^2(t - \tau)^2 V^{i-1}(t)d\tau\right\}\right\}. \qquad (9)$$

The calculation of V_{tot} is performed numerically. The best fitting results generated require that the initial set of nucleating islands be 5 AlN monolayers deep for sample A and 3 monolayers deep for sample C, shown as solid lines in Figs. 4(a) and 10, respectively. These thicknesses are determined in the fitting process by the positions of the crossover between the two growth regimes identified above.

The fitting results and some important parameters calculated are shown in Table IV. The final domain sizes are calculated from the AlN peak widths of the GID radial scans. The top layer nucleation densities N are estimated from the final domain sizes. These are used together with the fitting results of the nucleation and growth model to obtain the values of lateral growth velocity ν_1 of the initial nucleating islands, the lateral growth velocity ν_2 of subsequent sublay-

TABLE IV. Fitting results and calculations of nucleation and growth model.

Nitridation temperature (°C)	Thickness of the initial nucleating islands (ML)	Final domain size (nm)	N Initial layer nucleation density (cm^{-2})	M Subsequent layer nucleation rate (cm^{-2} s^{-1})	ν_1 Initial layer growth rate (nm/s)	ν_2 Subsequent layer growth rate (nm/s)
300	5	14.6	4.7E+11	9.4E+10	0.10	0.017
750	3	15.0	4.4E+11	8.1E+11	0.15	0.050

ers, and the nucleation rate M of the subsequent sublayers.

We consider why nucleating islands are initially several monolayers thick. Results of x-ray crystal truncation rod (CTR) measurements by G. Renaud *et al.*[20] suggest that the unreconstructed sapphire surface is terminated by a single layer of Al atoms, which is also energetically favored according to calculations. Theoretical calculations of the energetics of AlN layers on sapphire indicate that N atoms substitute for the O atoms in the basal planes of sapphire, rather than binding to the top terminating Al layer.[21] It is possible that, once AlN nucleates in the underlayers, the local chemistry around it is modified and N atoms can directly bind to the top Al surface, which may explain the growth of multiple layers together. Another possibility is a scarcity of nucleation sites, which could allow the extended downward growth of the AlN islands for several monolayers before the time that their lateral growth causes them to impinge.

B. High temperature nitridation—growth kinetics

Cho *et al.*[11] studied the growth of the nitrided layer at 700 °C with XPS and concluded that their data could be fit by a $\sqrt{t}$ growth law, which suggests a diffusion-limited growth. However, our detailed early-stage growth data could not be fit by a simple square-root growth function, shown as a dashed line in Fig. 4(b). On the other hand, our high temperature nitridation data can be fit moderately well by the nucleation model described above. The fitting result of the AlN ($10\bar{1}0$) peak evolution (see Table IV) gives a best fit when using three AlN monolayer in the nucleating islands; this fit is shown as a solid line in Fig. 4(b). This is consistent with the electron density evolution from reflectivity fitting shown in Fig. 5. However the lack of much structure in the experimental growth curve makes a definitive statement about the structure of nucleating islands more difficult than is the case for the low temperature nitridation.

C. Comparison of high- and low-temperature growth kinetics

We see from the fit results that the initial nucleation densities at the high and low temperatures are approximately equal, suggesting that nucleation on the sapphire surface occurs at specific sites whose density is temperature independent. The lateral growth rates of the initial layer at the high and low temperatures are also similar, which implies that the rate of arrival of active nitrogen species at the surface may be a limiting factor during growth of the first layer. The lateral growth rate of subsequent layers is approximately 6

times (for low temperature nitridation) and 3 times (for high temperature nitridation) slower than the lateral growth rate of the initial AlN islands, as might be expected since diffusion through the initial layer is required. The results suggest that the primary factors increasing the overall film growth rate at higher temperatures are increases in the rates of the formation of subsequent layers and their lateral growth. This is consistent with sublayer growth being controlled by thermally activated processes such as diffusion and reaction. Simple calculations with the fit rate constants suggest that activation energies are in the range of 0.1–0.25 eV.

D. Strain relaxation

It has been reported by Kim *et al.*[22] that the strain of a AlN layer on sapphire is fully relaxed after it grows thicker than 500 Å. In our case, the nitrided layer is much thinner (<25 Å), and remains compressively strained. It is also mentioned by Ng *et al.*[23] and Woll *et al.*[24] that the AlN formed by the nitridation process is under extreme compressive stress. In our studies, strains calculated from the AlN ($10\bar{1}0$) peak positions show that the initial and final strains for low and high temperature are similar. The final strains are approximately 1.4–1.5% relative to the bulk AlN value. This is in close agreement with the strain of 1.3% found by Woll *et al.* for a nitride formed by plasma nitridation at 1000 °C.

The large mismatch between AlN and sapphire suggests that the interface between the two will not be coherent. Indeed, the formalism of Bourret *et al.*,[25] which assumes the existence of a coherent interface with mismatch strain relaxing elastically during subsequent layer growth, significantly underestimates the overall strain relaxation. It predicts AlN strains decreasing only from 11.9% to 7.6% as the film grows from 1 to approximately 6 MLs, far larger than the observed strains.

In their studies of the nitridation of sapphire at 1000 °C, Woll *et al.*[24] found that the nitrided layer [$10\bar{1}0$] exhibited ±2° rotations relative to the sapphire [$11\bar{2}0$]. This may help reduce the effective mismatch strain between the nitride and the sapphire, in a similar manner to that observed in the bare sapphire $(\sqrt{31} \times \sqrt{31})R \pm 9°$ reconstruction. Indeed, the initial AlN domain sizes observed here are roughly comparable to the domain sizes in the $(\sqrt{31} \times \sqrt{31})R \pm 9°$ reconstruction. On the other hand, the x-ray rocking scans on the AlN ($10\bar{1}0$) peak performed during growth gave no sign of two distinct nitride island orientations. Thus the extent to which local

rotations may help relax the strain in the first nitride layer remains unclear.

E. External factors on nitridation

The differences in the nitridation rates and behaviors observed between samples A and C is unexpected. Since sample C is grown at a lower temperature, it might be expected *a priori* that it would exhibit slower growth because of the decrease in diffusion. Our experience, however, is that there can be several external factors which can play a significant role in the nitridation process.

The state of the nitrogen plasma may itself play a role. Previous studies[7,8] report that an RF plasma source produces nitrogen atoms, excited neutral nitrogen molecules, and a small fraction of ionized molecular nitrogen. Though both molecules and atoms are quite reactive and participate in the incorporation of N into the growing material, the metastable molecular nitrogen ions are more active and crucial to the nitridation. The concentration of each active nitrogen species at a certain level of energy may vary each time the plasma is initiated.

Chamber cleanliness and the purity of the nitrogen gas can also significantly affect the nitridation process. In the presence of impurities, the nitridation rate slows considerably or the process can even stop. When the nitrogen gas purifier is not used, for instance, we observe no AlN peaks in the GID or RHEED patterns. Yet, reflectivity curves still indicate that a thin film is growing with a density approximately 20% smaller than the bulk AlN value. This suggests that in the presence of impurities, such as oxygen, an amorphous layer may form and hinder the growth of a crystalline AlN layer. The amorphous layer might be AlO_xN_{1-x} which has a smaller electron density than pure AlN, as observed.

The incorporation of residual oxygen may play a role even in cases of apparently successful nitridation. It has been reported[26] from extended x-ray absorption fine structure measurements that, in the presence of oxygen contamination, oxygen impurity atoms substitute for N atoms in the N sublattice. Due to the shorter bond length of Al−O (0.167 nm) relative to that of Al−N (0.185 nm), the lattice parameter of AlO_xN_{1-x} is expected to be smaller than that of AlN. Therefore oxygen in the AlN film may cause the lattice parameter in the nitrided layer to be slightly smaller than expected, giving the same effect as compressive mismatch stress.

V. CONCLUSIONS

In summary, low and high temperature nitridation of (0001) sapphire assisted by RF nitrogen plasma source was studied by RHEED, x-ray reflectivity, and real-time GID. The initial nitridation at both low and high temperatures occurs through a nucleation and growth process. At low temperature, nitridation either saturates or continues at a slower rate after the growth of initial nucleating islands which are a few AlN monolayers thick. This is consistent with the need for diffusion through the existing nitride layer for further growth. However, at high temperature, diffusion through the existing nitride layer is apparently sufficiently fast that, in the early time regime examined, nitridation proceeds without much slowdown following completion of the first layer. The similarity of lateral domain sizes during low and high temperature growths suggests that the nucleation density of initial layers is similar in the two cases and likely due to nucleation on a fixed density of active sites. The site nucleation density of approximately 4×10^{11} cm^{-2} is comparable to the density of dislocations in typical epilayer films. The lateral growth velocity of the initial layers at high temperature is similar to that at low temperature, implying that the rate of active nitrogen species arrival at the surface could play a limiting role during this part of the nitridation process. However, the rate of growth of subsequent sublayers is much higher at high temperature than at low temperature, consistent with thermally activated energies for diffusion or reaction of a few tenths of an electron volt. The presence of impurities during nitridation may cause the formation of amorphous structures, such as AlO_xN_{1-x} compounds and inhibit the formation of the crystalline AlN.

ACKNOWLEDGMENTS

[1] T. D. Moustakas, R. J. Molnar, T. Lei, G. Menon, and C. R. Eddy, Mater. Res. Soc. Symp. Proc. **242**, 427 (1992).

[2] T. D. Moustakas, T. Lei, and R. J. Molnar, Physica B **185**, 36 (1993).

[3] D. Doppalapudi, E. Iliopoulos, S. N Basu, and T. D. Moustakas, J. Appl. Phys. **85**, 3582 (1999).

[4] F. Widmann, G. Feuillet, B. Daudin, and J. L. Rouviere, J. Appl. Phys. **85**, 1550 (1999).

[5] Gon Namkoong, W. Alan Doolittle, April S. Brown, Maria Lo-surdo, Pio Capezzuto, and Giovanni Bruno, J. Vac. Sci. Technol. B **20** (3), 1221 (2002).

[6] Ki-Sung Kim, Seon-Hyo Kim, and Dong-Ryul Lee, Appl. Phys. Lett. **76**, 1552 (2000).

[7] E. Iliopoulos, A. Adikimenakis, E. Dimakis, K. Tsagaraki, G. Konstantinidis, and A. Georgakilas, J. Cryst. Growth **278**, 426 (2005).

[8] A. J. Ptak, M. R. Milecchia, T. H. Myers, K. S. Ziemer, and C. D. Stinespring, Appl. Phys. Lett. **74**, 3836 (1999).

[9] C. Heinlein, J. Grepstad, T. Berge, and H. Riechert, Appl. Phys. Lett. **71**, 341 (1997).

[10] K. Uchida, A. Watanabe, F. Yano, M. Kouguchi, T. Tanaka, and S. Minagawa, J. Appl. Phys. **79**, 3487 (1996).

[11] Y. Cho, Y. Kim, E. R. Weber, S. Ruvimov, and Z. L. Weber, J. Appl. Phys. **85**, 7909 (1999).

[12] F. Dwikusuma and T. F. Kuech, J. Appl. Phys. **94**, 5656 (2003).

[13] A. S. Ozcan, G. Ozaydin, Y. Wang, K. F. Ludwig, R. L. Headrick, H. Zhou, and D. P. Siddons (unpublished).

[14] T. Lei, K. F. Ludwig, Jr., and T. Moustakas, J. Appl. Phys. **74**, 4430 (1993).

[15] Michael F. Toney and Carol Thompson, J. Chem. Phys. **92**, 3781 (1990).

[16] G. Renaud, Surf. Rev. Lett. **7**, 437 (2000).

[17] J. W. Christian, *The Theory of Transformations in Metals and Alloys*, 2nd ed. (Pergamon, Oxford, 1981), Part I.

[18] Kenneth A. Jackson, *Kinetic Processes: Crystal Growth, Diffusion, and Phase Transitions in Materials* (John Wiley & Sons, New York, 2004).

[19] M. A. Singh, C. R. Harkless, S. E. Nagler, R. F. Shannon, Jr., and S. S. Ghosh, Phys. Rev. B **47**, 8425 (1993).

[20] G. Renaud, Surf. Sci. Rep. **32**, 1 (1998).

[21] R. Di Felice and J. E. Northrup, Appl. Phys. Lett. **73**, 936 (1998).

[22] J. W. Kim, Y. H. Hwang, J. H. Cho, and H. K. Kim, Jpn. J. Appl. Phys., Part 1 **40**, 4677 (2001).

[23] H. M. Ng, D. Doppalapudi, D. Korakakis, R. Singh, and T. D. Moustakas, J. Cryst. Growth **190**, 349 (1998).

[24] A. R. Woll, R. L. Headrick, S. Kycia, and J. D. Brock, Phys. Rev. Lett. **83**, 4349 (1999).

[25] A. Bourret, C. Adelmann, B. Daudin, J. L. Rouviere, G. Feuillet, and G. Mula, Phys. Rev. B **63**, 245307 (2001).

[26] M. Katsikini, E. C. Paloura, T. S. Cheng, and C. T. Foxon, J. Appl. Phys. **82**, 1166 (1997).